18,12

Composite based on multi-walled carbon nanotubes and manganese oxide doped with silver oxide for supercapacitors electrodes

© S.N. Nesov[1,2], I.A. Lobov[1], S.A. Matyushenko[1], V.V. Bolotov[1], K.E. Ivlev[1], D.V. Sokolov[1], Yu.A. Sten'kin[1]

[1] Omsk Scientific Center, Siberian Branch, Russian Academy of Sciences, Omsk, Russia
[2] Omsk State Technical University, Omsk, Russia

E-mail: nesov55@mail.ru

Received September 6, 2023
Revised September 6, 2023
Accepted September 18, 2023

A composite based on multi-walled carbon nanotubes and manganese oxide doped with silver oxide, promising as an electrode material for supercapacitors, has been obtained and studied. The structure and composition of the composite and electrodes obtained on its basis were studied by scanning electron microscopy and X-ray photoelectron spectroscopy. Using potentiostatic and galvanostatic methods, the characteristics of electrodes based on the composite, as well as combinations of the composite and commercial highly dispersed carbon black (CB) in various ratios, were studied. The most optimal characteristics were obtained for combined electrodes with CB contents of 20 and 30 wt.%: the specific capacitance values were $\sim 145-130$ F/g at a discharge current density of 0.1 A/g, maintaining 65% of this value when increasing the discharge current density to 1 A/g. Based on the analysis of morphology and electrophysical characteristics, it is shown that high electrochemical characteristics of combined electrodes are achieved through a combination of high electrochemical activity of the composite, as well as the electrical conductance and porosity of carbon black.

Keywords: conductivity, specific capacitance, redox reactions, electrochemical characteristics, X-ray photoelectron spectroscopy.

DOI: 10.61011/PSS.2023.11.57334.196

1. Introduction

Supercapacitors (SC) are energy storage devices, which occupy an intermediate position between capacitors and lithium-ion batteries in terms of their characteristics [1]. The specific capacitance and energy density of SCs significantly exceed the values typical for traditional capacitors. Compared to lithium-ion batteries, SCs have a higher specific power, significantly shorter charge/discharge times, and are also cheaper and more environmentally friendly, although they are noticeably inferior in terms of specific capacity [2]. SC electrodes are usually made of porous carbon material with a high specific surface area. Charge accumulation in an ideal SC occurs in an electrical double layer (EDL) that emerges at the contact interface between the electrodes and the electrolyte [3].

Pseudocapacitors (PC) are supercapacitors in which charge accumulation is realized not only due to the formation of a double electrical layer at the electrode–electrolyte interface, but also due to the reversible redox reactions proceeding with the involvement of the surface layer of the active material and electrolyte ions. The capacitance associated with the charge accumulated due to the running of electrochemical reactions is known as pseudocapacitance [4]. Oxides of various transition metals are used as active materials in PCs [1,4,5]. As a rule, they have a higher specific capacity compared to double-layer SCs, but at the same time they are significantly inferior in charge/discharge speed [5].

MnO_2 manganese oxide is one of the most promising transition metal oxides used as an active material for PC electrodes. This oxide has a high theoretical specific capacity, low cost, and high availability [4,5]. However, its significant disadvantage is low conductivity (of the order of $10^{-5}-10^{-6}$ Sm/cm), which limits its practical use [6]. One of the promising directions that makes it possible to effectively use MnO_2 as a PC electrode material is the creation of composites based on it in combination with various types of electrically conductive carbon nanostructured materials (nanotubes, nanofibers, graphene, etc.) [1–5]. The electrical conductance of manganese oxide can be further increased by doping it with metals and metal oxides that have high electrical conductivity. In [7], a significant improvement in the electrochemical characteristics of manganese oxide when doped with silver was reported. The conductivity of silver and its most stable oxide, Ag_2O (10^7 and 10^5 Sm/cm, respectively [8]) is several orders of magnitude higher than the value for MnO_2.

In our previous work, we investigated the structure and electrochemical characteristics of a composite based on multi-walled carbon nanotubes and manganese oxide ($MWCNT|MnO_x$) formed by soaking the MWCNT in an

Table 1. Composition of the active material of the electrodes and specific conductivities based on the results of four-probe measurements

Electrode	Active material composition	Specific conductivity, S/cm
CNT	MWCNT	0.480 ± 0.010
CB	Printex XE2-B CB	0.210 ± 0.020
K (100%)	MWCNT|MnO_x@AgO_y composite	0.005 ± 0.010
K (90%) CB (10%)	MWCNT|MnO_x@AgO_y composite + CB Printex XE2-B (9:1, mass)	0.025 ± 0.010
K (80%) CB (20%)	MWCNT|MnO_x@AgO_y composite + CB Printex XE2-B (8:2, mass)	0.032 ± 0.010
K (70%) CB (30%)	MWCNT|MnO_x@AgO_y composite + CB Printex XE2-B (7:3, mass)	0.104 ± 0.020

aqueous solution of $KMnO_4$ followed by high-temperature treatment in an inert atmosphere [9]. The specific capacity of the resulting composite was 3–5 times higher than the capacity of the initial MWCNTs. Using X-ray photoelectron spectroscopy, the presence of MnO_2 and Mn_2O_3 oxides in the composite was demonstrated. The presence of the latter is undesirable due to the higher resistivity [10]. In this study, the formation mode of the MWCNT|MnO_x composite was modified in order to increase the mass loading of the composite with the MnO_2 oxide. To increase the electrical conductivity of the composite, it was doped with silver oxide at the stage of synthesis. The resulting composite was investigated as an active component to improve the electrochemical performance of the carbon black.

2. Experiment

2.1. Forming the composite

The composite was formed using MWCNTs synthesized by chemical vapor deposition (CVD) (MWCNT-1 produced by the Institute of Catalysis of the Siberian Branch of RAS, Novosibirsk, Russia). The average diameter of MWCNTs was 7–7.5 nm and their specific surface area was $\sim 360 \pm 20\,m^2/g$. Initially, 500 mg MWCNTs were treated in 0.5 M HNO_3 for 5 min to improve hydrophilic properties. Then the MWCNTs were washed repeatedly in distilled water until the remaining acid was completely removed. The treated MWCNTs were placed in a solution containing 1 g of $KMnO_4$, 50 mg of $AgNO_3$, and 75 ml of distilled water. The resulting suspension was kept at a temperature of 60°C and atmospheric pressure for 48 h. The resulting MWCNT|MnO_x@AgO_y composite (black powder) was washed repeatedly in distilled water, followed by drying at a pressure of $\sim$ 1 Pa and a temperature of 80°C for 6 h.

2.2. Forming the electrodes and electrochemical measurements

The MWCNT|MnO_x@AgO_y composite was investigated as a basis for the fabrication of PC electrodes and also as an active component for improving the electrochemical performance of carbon black (CB). The Printex XE2-B CB was used, which has high electrical conductivity and a specific surface area of $\sim 1000\,m^2/g$. Polyvinylidene fluoride (PVDF) was used as a binder to fabricate electrodes. Initially, the active material (composite or a mixture of composite and CB) was mixed with PVDF in proportions of 9:1 (by weight) followed by the addition of 1-methyl-2-pyrrolidone (NMP) until a homogeneous suspension was formed. Then, after prolonged stirring, the resulting mass was dried at a temperature of 50°C to partially remove the NMP, and then, using a roller, it was rolled into a plate with a thickness of $\sim 100\,\mu m$. The finally formed 10×15 mm electrodes were dried for 6 h at a temperature of 90°C and a pressure of $\sim$ 1 Pa. Symbols of the electrodes prepared for the study, the composition of their active mass, as well as values of conductivity determined from the results of four-probe measurements are presented in Table 1. It is important to note that a composite containing metal oxides has a significantly higher density compared to CB. Therefore, when these materials were mixed in a mass ratio of 9:1, their volume ratio was visually assessed as close to 1:1. Even at a mass ratio of 8:2, the volume fraction of the composite was less than the volume fraction of CB.

The electrochemical characteristics of the electrodes were analyzed using the methods of cyclic voltammetry (CV), as well as galvanostatic charge–discharge. For this purpose, a P-40X potentiostat-galvanostat unit (Elins, Zelenograd, Russia) was used. The measurements were carried out using a three-electrode scheme with a 10×15 mm platinum plate as a counter electrode. A standard Ag|AgCl|KCl electrode was used as a reference electrode, which was placed in an electrochemical cell using a Luggin capillary. The working electrode was also placed on a 10×15 mm platinum plate

using a fluoroplastic clamping device. 1 M aqueous solution of Na_2SO_4 was used as an electrolyte. Specific capacitance (C_s) was calculated from the results of galvanostatic measurements as: $C_s = (I\Delta t)/(Um)$, where I is discharge current, Δt is discharge time, U is window of potential (0.8 V), m is mass of active material in the electrode. Before the measurements, the electrodes were kept in the electrolyte for about 48 hours, and then stabilized in CV mode at a potential sweep rate of 20 mV/s for 100 charge-discharge cycles in an electrochemical cell.

2.3. Analysis of structure, morphology, elemental composition, and chemical state

To analyze the structure, morphology, and elemental composition of the composite and fabricated electrodes, a JSM 6610-LV scanning electron microscope (SEM) equipped with an INCA-350 Oxford Instruments attachment for X-ray energy dispersive analysis (EDX) was used. The accelerating voltage when studying samples using scanning electron microscopy was 20kV. The depth of analysis of porous carbon samples by the EDX method can reach 10 μm or more.

The chemical state of the resulting composite was analyzed by X-ray photoelectron spectroscopy (XPS) with a source of nonmonochromatic AlK_α-radiation. XPS spectra were recorded at ultrahigh vacuum in the analysis chamber (with a pressure of $\sim 10^{-7}$ Pa). The area of the X-ray beam was $\sim 3\,mm^2$, and the source power was 240 W. Energy resolution when recording core line spectra was ~ 0.2 eV, and that of survey spectra was ~ 1.2 eV. The effective analysis depth by this method is several orders of magnitude less than the EDX depth and amounts to ~ 5 nm.

3. Results and discussion

3.1. Structure and chemical state of the composite

Figure 1 shows SEM images of the formed MWCNT|MnO_x@AgO_y composite. In the images of the composite (Figure 1, *a*) large particles with sizes up to $\sim 10\,\mu$m are observed (shown with number *1* in Figure 1, *a*). The high brightness of these particles suggests that they contain a large amount of manganese oxide, the density of which is significantly higher than the density of carbon nanotubes. The image contrast is also affected by the low electrical conductance of manganese oxide. The cylindrical agglomerates shown with number *2* in Figure 1, *a* are probably bundles of MWCNTs coated with layers of manganese oxide. Analysis of a detailed SEM image of one of the particles (Figure 1, *b*) shows the presence of tubular structures on its surface (shown with number *3*), which may be fragments of MWCNTs, that allows supposing the presence of carbon nanotubes in the volume of these particles. However, the bulk of the composite consists of MWCNTs, the surface of which is covered with layers of manganese oxide (Figure 1, *c*). These MWCNTs are randomly oriented and have multiple crossings similar to carbon nanotubes in unoriented arrays.

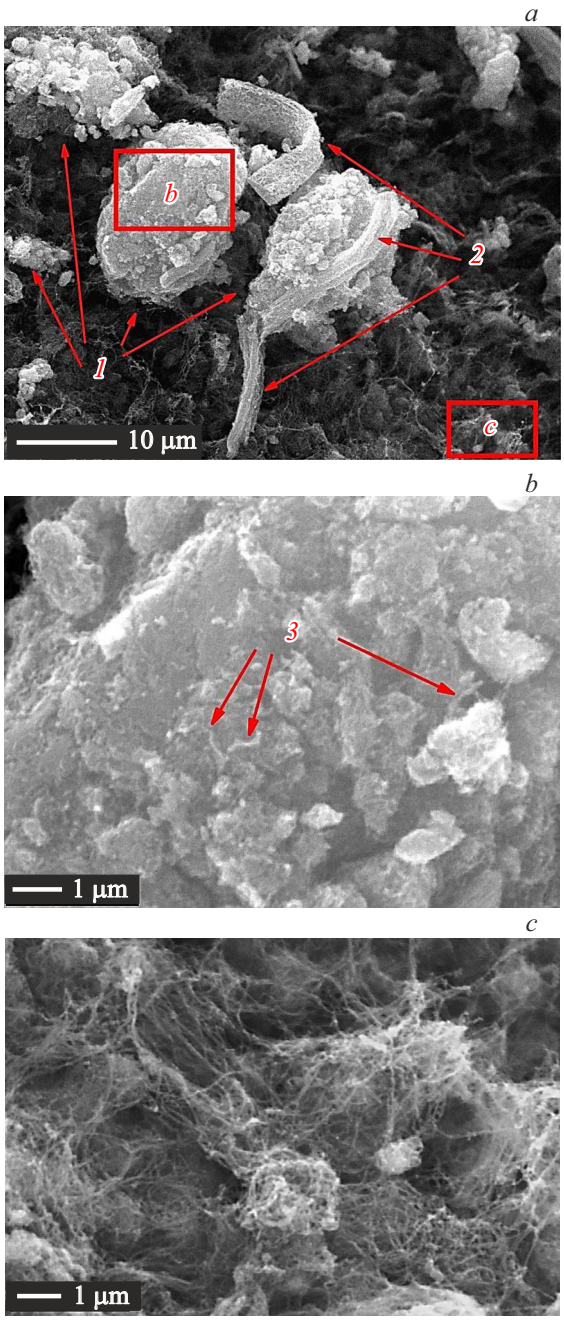

Figure 1. *a* — SEM image of the MWCNT|MnO_x@AgO_y composite; *b* — zoomed-in image of the area *b* in Figure 1, *a*; *c* — zoomed-in image of the area *c* in Figure 1, *a*. The numbers indicate: *1* — metal oxide particles, *2* — bundles and strands of MWCNTs, *3* — fragments of MWCNTs in the composition of metal oxide particles.

Analysis of the elemental composition by EDX is presented in Table 2. The results of elemental analysis indicate a fairly uniform distribution of manganese and silver in the composite.

Table 2. Elemental analysis of the composite at various points based on the EDX data

Point number	Concentration, at.%				
	C	O	Mn	Ag	K
1	38.4	40.6	15.9	0.8	4.3
2	32.2	42.2	19.4	0.9	5.2
3	32.4	45.5	16.8	0.8	4.5
4	27.1	49.5	17.9	1.0	4.5
Average value	32.6	44.4	17.5	0.9	4.6

The presence of potassium in the composite in the form of residues of $KMnO_4$, as well as products of its decomposition (K_2MnO_4, K_3MnO_4) is unlikely because these compounds are unstable in water and are easily removed by repeated washing. It is most likely that potassium is present as an impurity in the manganese dioxide ($K_{2-x}Mn_8O_{16}$) [11]. The high oxygen content in the results of EDX analysis indicates the oxidized state of the metals and the MWCNT surface in the composite.

The survey XPS spectrum of the formed composite (Figure 2, *a*) contains lines of manganese, oxygen, carbon, silver and potassium. The results of quantitative elemental analysis carried out on the basis of survey spectrum using the method of elemental sensitivity coefficients (presented in the table in Figure 2, *a*). The discrepancy between the results of quantitative analysis of the composite based on the EDX and XPS data is probably due to a significant difference in the depth of analysis for these methods ($\sim 10\,\mu$m for EDX and ~ 5 nm for XPS). The high oxygen concentration in the results of quantitative XPS analysis is indicative of the oxidation of the MWCNT surface in the process of composite formation. It should be noted that in our previous study [9] the proportion of manganese in the composite formed at room temperature was only ~ 8 at.% according to XPS data. The mode of composite formation proposed in this study provides a higher mass loading of the composite with manganese oxide.

The chemical state of manganese was analyzed using XPS spectra of Mn2*p* and Mn3*s*. The position of the $Mn2p_{3/2}$ maximum is ~ 642.4 eV, and the energy distance between the $2p_{3/2}$ and $2p_{1/2}$ lines is 11.8 eV (Figure 2, *b*), which according to [12,13] corresponds to the MnO_2 oxide. According to [12,14], the energy distance between the maxima in Mn3*s* is almost independent of the effect of surface charging and is 5.3–5.5 eV for Mn^{3+} states and 4.7–4.5 eV for Mn^{4+} states. In our case, the splitting of the Mn2*s* doublet is 4.6 eV (Figure 2, *c*). This confirms that the main part of manganese in the composite is present in the form of MnO_2.

In the range of binding energies of 300–280 eV (Figure 2, *d*) there are the line C1*s* (~ 285.0 eV), as well as the doublet line K2*p* (298–291 eV). The full width at half maximum (FWHM) of the line C1*s* is 2.46 eV, which is significantly larger compared to this value in the spectrum of the initial MWCNTs (1.59 eV), measured under similar conditions [9]. This is indicative of a significant oxidation of the outer walls of carbon nanotubes and an increase in the number of structural defects in them during the formation of the composite. According to [15], the maximum of states corresponding to the sp^2-hybridized carbon is located at the binding energy of ~ 284.5 eV. The binding energy range of ~ 285 eV corresponds to carbon states with sp^3-hybridization of valence orbitals ($C-C(sp^3)$), as well as the states of carbon atoms located close to the oxygen groups pinned at the surface of MWCNT ($C^*-C(O)$). The binding energy ranges of ~ 286.5, ~ 288.5, and ~ 289.5 eV correspond to the states of carbon in the C–O, C=O, and O–C=O bonds, respectively [16]. As can be seen from the results of decomposition of the carbon spectrum (Figure 2, *d*), the components corresponding to structural defects, as well as to the carbon in various functional groups, have high intensity. These results suggest the possible formation of chemical bonds between manganese oxide and the defective oxidized surface of MWCNTs at the composite interfaces.

Figure 2, *e* shows the XPS spectrum of the Ag3*d* line, which partially overlaps with the K2*s* line. The main maximum of $Ag3d_{5/2}$ is well approximated by one component with a maximum at the binding energy of ~ 368.0 eV, which, according to the literature data, can correspond to both metallic silver and Ag_2O silver oxide [17]. However, taking into account that the synthesis of the composite is carried out in an oxidizing environment, we believe that silver in the composite is present in the form of Ag_2O oxide.

3.2. Analysis of the structure and electrochemical characteristics of electrodes

Figure 3, *a* shows a SEM image of the K (100%) electrode. It can be seen that the electrode has a globular structure: porous globules of irregular shape up to several μm in size are observed, which presumably are agglomerates of intertwined randomly oriented MWCNTs. The agglomerates are separated by voids of $\sim 1\,\mu$m in size. Most of the agglomerates have a porous structure formed by intertwined carbon nanotubes with pore sizes of the order of several tens of nanometers. Some globules contain denser, nonporous regions, which are presumably manganese oxide particles or clusters of MWCNTs coated with massive metal oxide layers. The structure of the CB electrode is shown in Figure 3, *b*. In this case, carbon black forms a denser, homogeneous medium, where presumably macropores, mesopores, and micropores are concurrently present.

In the structure of the K (90%) CB (10%) electrode there is the presence of fairly large areas with a morphology typical for the K (100%) electrode (upper region in Figure 3, *c*), as well as areas with a morphology typical for the CB electrode (lower part in Figure 3, *c*). However, in this

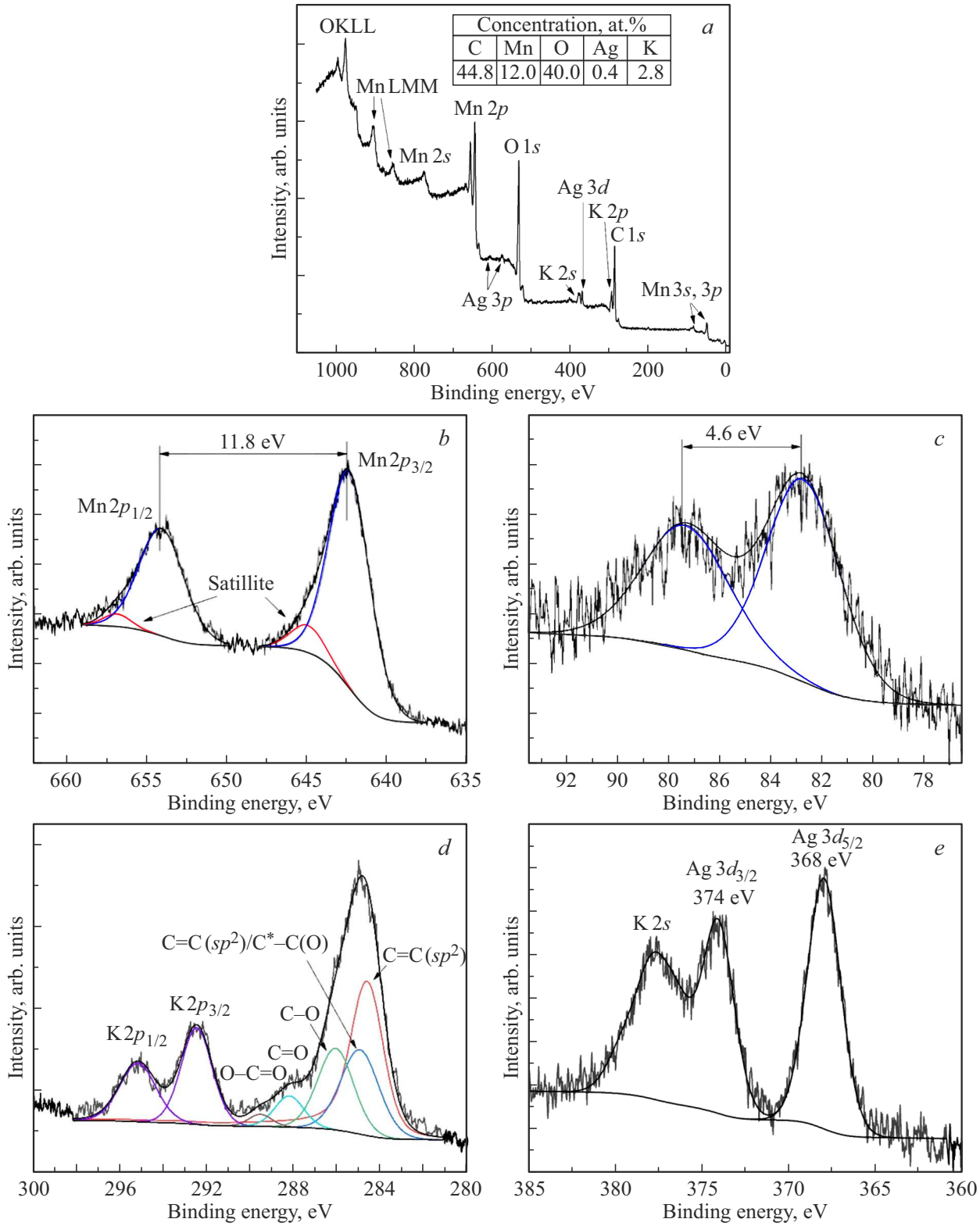

Figure 2. XPS spectra of the MWCNT|MnO_x@AgO_y composite: *a* — survey spectrum (the inset shows the results of elemental analysis); *b* — Mn2*p*; *c* — Mn3*s*; *d* — C1*s* (overlap with K2*p*); *e* — Ag3*d* (overlap with K2*s*).

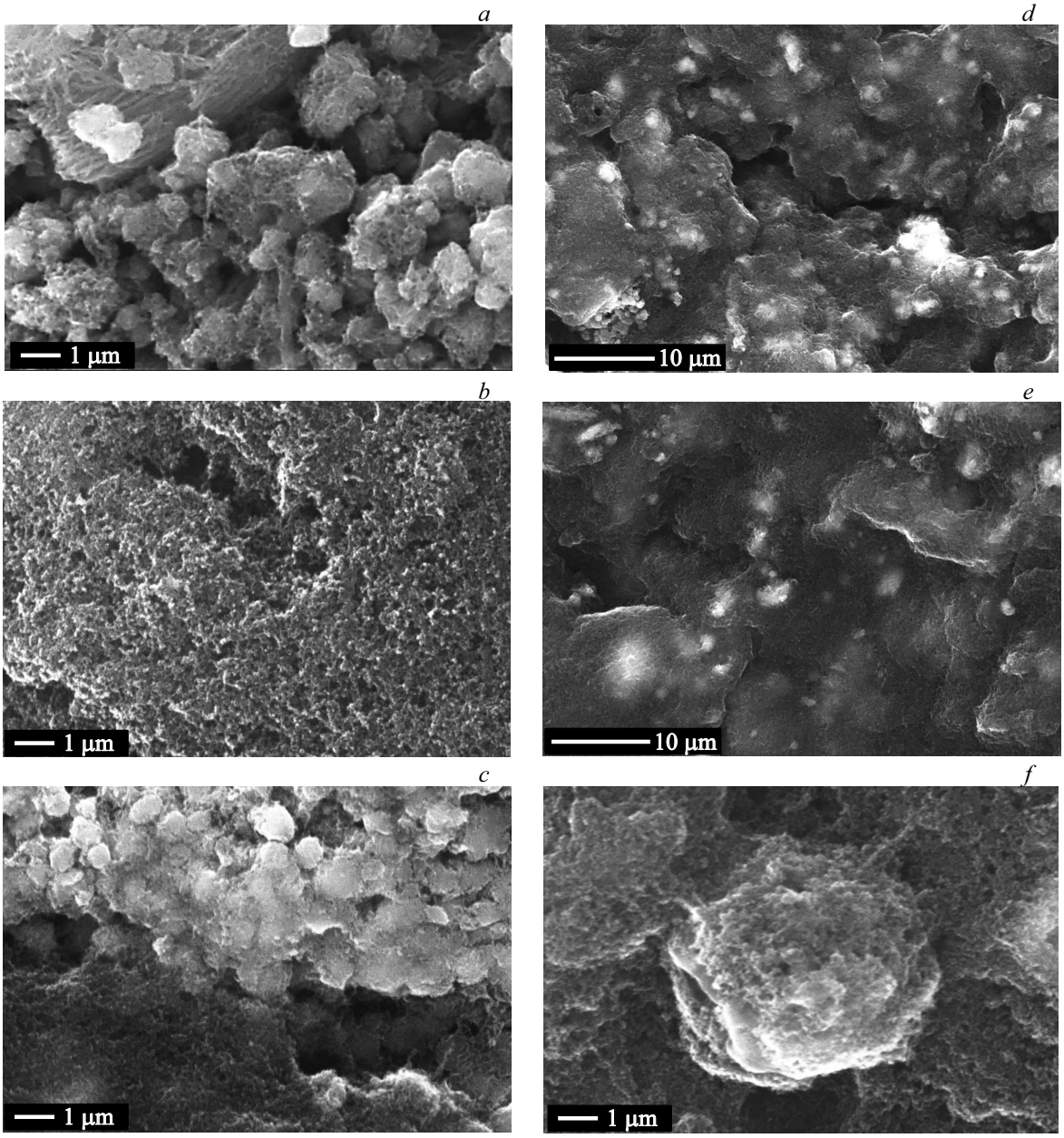

Figure 3. SEM images of electrodes: *a* — K (100%); *b* — CB; *c* — K (90%) CB (10%); *d* — K (80%) CB (20%); *e* and *f* — K (70%) CB (30%) at different magnification.

case, in areas consisting predominantly of CB, there are bright contrasting areas, which presumably are agglomerates of the composite in the bulk CB.

In K (80%) CB (20%) and K (70%) CB (30%) electrodes (Figure 3, *d*–*f*) there is a fairly uniform distribution of composite agglomerates (light areas) in the porous matrix formed by carbon black (dark areas). At the same time, a series of images obtained at high magnifications makes it possible to state that the major portion of the composite agglomerates is located in the volume of the matrix formed by carbon black (Figure 3, *f*). It is also clearly visible (Figure 3, *d*–*e*) that even at a mass content of carbon black of 20% it is the carbon black that forms the main volume of the electrode.

3.3. Analysis of electrochemical characteristics of electrodes

To analyze the mechanisms of charge accumulation in electrodes based on the materials under study, the CV method was used. Volt-amperograms of CNT and CB electrodes have a quasi-rectangular shape, which is typical for carbon materials that accumulate charge due to the formation of EDL [18]. The areas of the CV curves of

these electrodes are approximately equal, which indicates similar capacitive characteristics of these materials. The slight asymmetry of the CV curves of these electrodes is presumably due to the presence of oxygen-containing functional groups in their composition [19]. The CV curves of electrodes containing the MWCNT|MnO_x@AgO_y composite outline noticeably larger areas, which is indicative of higher capacitance of the electrodes compared to CNT and CB electrodes. It is obvious that the increase in capacitance is ensured by the proceeding redox reaction [20]:

$$MnOOM_x^+ + nSO_4^{2-} \leftrightarrow MnO_2//(SO_4)_n^{2-} + xM^+ + xe^-, \quad (1)$$

where M^+ are Na^+ cations from the electrolyte or K^+ cations (present in the composite according to EDX and XPS data), and the // symbol means electrical double layer. It is also possible for redox reaction to run with the participation of silver oxide present in the composite. In this case, the CV curve of the K (100%) electrode has an ellipsoidal shape (Figure 4, *a*), which may be due to the low electrical conductivity of the material (see Table 1). CV curves for electrodes containing the composite and CB in different mass proportions have a quasi-rectangular shape, which indicates higher electrical conductivity, as well as accessibility of the electrode surface for electrolyte ions. The volt-amperogram of the K (90%) CB (10%) electrode is not shown in Figure 4, *a* to avoid overlap of curves, because the shape and area are nearly the same as those of the CV curve of the K (80%) CB (20%) electrode.

The analysis of the capacitive characteristics of the electrodes was carried out by the galvanostatic charge−discharge method at different current densities in a range of 0.1−1 A/g. Due to the fact that the analyzed electrodes have pseudo-capacitance (i. e. they accumulate energy due to redox reactions, which are rather slow diffusion processes), they may not be fully charged in the direct current mode upon reaching the maximum potential (especially at high current densities). Therefore, in this study, two specific capacitance values were determined: when the cell was discharged immediately after its charging in the direct current mode (C_{s1}), and also after additional charging of the electrode in the potentiostatic mode for 300 s (C_{s2}). The scheme of such measurements is presented in Figure 4, *b* using the example of the charge-discharge curve of the K (100%) electrode at a current density of 0.2 A/g. It can be seen that the discharge time t_2 after an additional charging at DC voltage is longer than the time t_1 of discharge performed immediately after charging in direct current mode.

The discharge curves presented in Figure 4, *c* and *d* show that electrodes containing both composite and carbon black demonstrate a longer discharge time compared to the electrode prepared only on the basis of the composite. The capacitance characteristics of the analyzed electrodes calculated from the discharge curves are presented in Table 3. It should be noted that the specific capacitance (C_{s1}) of the MWCNT-based electrode was previously measured under similar conditions [9] and amounted to ∼ 20−15 F/g in the charge/discharge current density range of 0.1−1 A/g. As can be seen from Table 3, electrodes containing a mixture of composite and carbon black in various proportions demonstrate similar specific capacitance values (C_{s2}) at a current density of 0.1 A/g (∼ 144−129 F/g). The specific capacitance of the K (100%) electrode at a given current density is 30−40% lower than these values (∼ 107 F/g). The maximum value of the specific capacitance at a low charge/discharge current density is demonstrated by the K (80%) CB (20%) electrode.

With increasing charge/discharge current density, the specific capacitance values for all electrodes decrease (Table 3). This reduction can be quantitatively characterized using the *R* parameter presented in Table 3, which is the ratio of specific capacitances (C_{s2}) measured at current densities of 0.1 and 1 A/g. It can be seen that the K (100%) electrode retains less than 20% of capacitance (C_{s2}) when the current increases by a factor of 10. This, first of all, may be a consequence of insufficient electrical conductivity of the material and low accessibility of its surface for electrolyte ions. This is also indicated by a significant voltage drop (∼ 350 mV) observed during the transition from charge to discharge mode for a given electrode (indicated as ΔU in Figure 4, *d*). This voltage drop is directly proportional to the total equivalent resistance of the cell [21], which in this case consists of the resistance of the electrode material, electrolyte, as well as the resistance at the „electrode−electrolyte“ interface. The latter is mainly determined by the accessibility of the electrode surface to electrolyte ions. It is also worth noting the significant difference between the values of C_{s1} and C_{s2} measured at a current density of 1 A/g for the K (100%) electrode (Table 3), which is associated with the predominantly pseudo-capacitive mechanism of charge accumulation due to the proceeding redox reaction.

For the electrodes containing the composite and the carbon black, with an increase in the proportion of the latter in the electrode composition, an increase in the *R* parameter is observed (Table 3). Also, with an increase in the CB quantity, a decrease in the magnitude of the voltage drop at the beginning of the discharging is observed (Figure 4, *d*): for the K (90%) CB (10%) electrode this value is ∼ 160 mV, and for K (80%) CB (20%) and K (70%) CB (30%) electrodes it is ∼ 100 mV. According to the results of four-probe measurements (Table 1), electrodes with 10 and 20% mass. CB contents have similar conductivity values. Consequently, an increase in the proportion of CB from 10 to 20% mass. ensures a reduction in the equivalent resistance of the cell (directly proportional to the voltage drop ΔU) precisely due to the improved accessibility of the surface for electrolyte ions.

Coincidence of ΔU values for K (80%) CB (20%) and K (70%) CB (30%) electrodes (Figure 4 *d*) suggests that an increase in the mass fraction of CB from 20 to 30% does not lead to an increase in the accessibility of the surface for

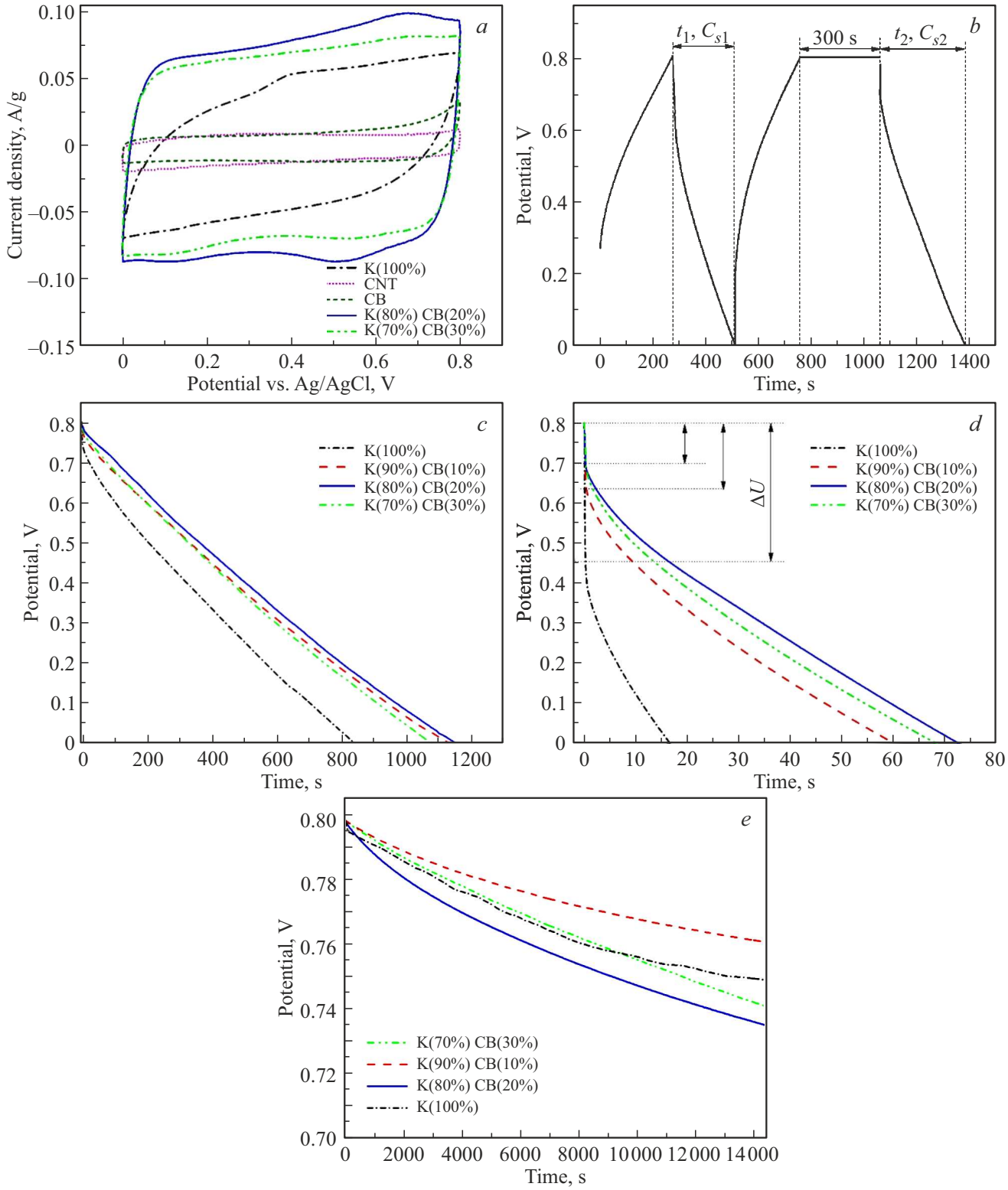

Figure 4. Electrochemical characteristics of electrodes. *a* — CV curves of the electrodes, measured at a potential sweep rate of 0.5 mV/s; *b* — charge–discharge curve of the K (100%) electrode at a current density of 0.2 A/g; *c* and *d* — discharge curves of electrodes at current densities of 0.1 and 1 A/g, respectively, *e* — self-discharge curves of electrodes with different contents of carbon black. (The curves presented in Figure 4, *c*–*e* were measured after an additional charging in the potentiostatic mode).

Table 3. Capacitive characteristics of electrodes with different contents of composite and carbon black when the charge/discharge current density changes

Current density, A/g	Specific capacitances C_{s1} and C_{s2} for electrodes, F/g									
	Electrode K (100%)		Electrode K (90%) CB (10%)		Electrode K (80%) CB (20%)		Electrode K (70%) CB (30%)		Electrode CB	
	C_{s1}	C_{s2}	C_{s1}	C_{s2}	C_{s1}	C_{s2}	C_{s1}	C_{s2}	C_{s1}	C_{s2}
0.1	96.4	107.3	135.9	141.8	135.0	144.3	129.3	134.7	20.1	20.2
0.2	57.0	80.5	116.7	131.5	122.0	139.1	117.2	129.4	19.2	19.4
0.3	40.1	66.4	105.8	126.3	123.0	130.5	106.3	122.6	18.4	18.7
0.4	34.5	57.3	95.0	120.6	100.2	126.0	87.9	120.1	16.9	17.8
0.5	23.6	51.5	84.3	114.6	93.8	112.6	84.4	117.2	15.1	16.5
1.0	2.25	20.8	31.5	75.4	44.3	90.2	43.8	87.8	12.3	15.4
$^*R$, %	19.1		53.2		62.5		65.2		76.2	

Note. $^*R$ is ratio of specific capacitances (C_{s2}) measured at current densities of 0.1 and 1 A/g.

electrolyte ions, although it provides a fourfold increase in conductivity (Table 3).

Also, it can be seen from the data in Table 3 that at a high discharge current density (1 A/g) the K (80%) CB (20%) and K (70%) CB (30%) electrodes demonstrate maximum and almost identical values of specific capacitance ($C_{s2} \sim 90$ F/g). In this case, a conclusion can be made that the effect of a fourfold increase in the specific conductivity of the electrode material on the specific capacitance is leveled out by a decrease in the proportion of the electrochemically active component (the composite) in the electrode composition with an increase in the mass fraction of the CB from 20 to 30%. At the same time, from an economic point of view, increasing the share of CB is beneficial, because it reduces the cost of the material.

Figure 4, *e* shows the results of the analysis of the self-discharge characteristics of the electrodes. The decrease in voltage in the cell over 4 h for the composite-containing electrodes is $\sim 40-60$ mV or $\sim$ 5–8% of the initial voltage (0.8 V). For CB and CNT electrodes, the decrease in voltage when analyzing self-discharge (curves not shown in the figures) is ~ 300 mV for only 1 hour.

The data obtained on the morphology, as well as the electrophysical and electrochemical characteristics of the electrodes indicate a synergistic effect arising from combining the properties of the MWCNT|MnO_x@AgO_y composite and carbon black, which manifests in an increase in specific capacity and stability of capacitive characteristics with increasing discharge current density. The essence of this effect can be revealed by referring to Figure 5, which schematically shows the process of charging the electrodes based on the composite (Figure 5, *a*), as well as on a mixture of the composite and highly dispersed porous CB (Figure 5, *b*). In the case of the composite-based electrode, charge accumulation occurs mainly due to the proceeding redox reaction. According to the SEM data, the composite-based electrode is represented by a set of micrometer-sized agglomerates consisting of MWCNT and

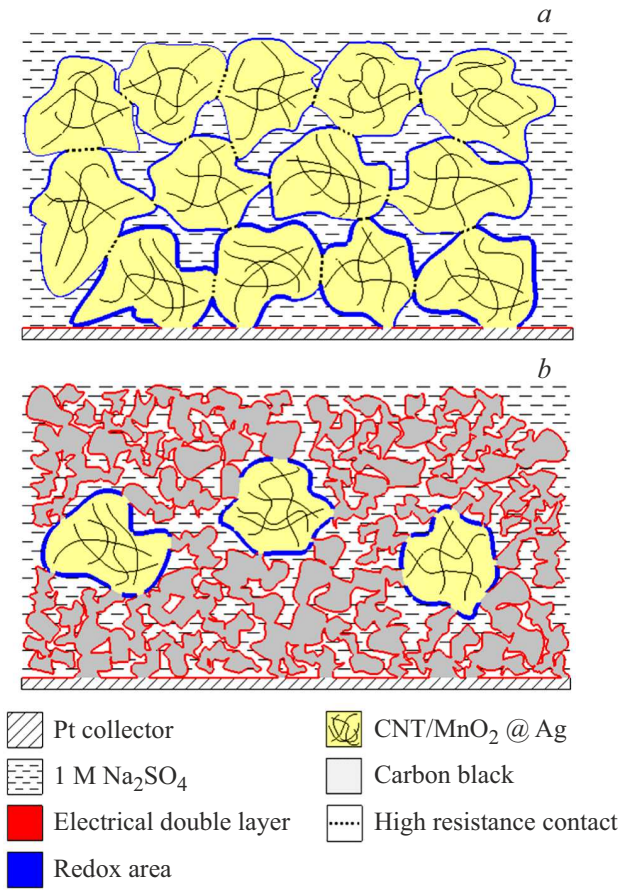

Figure 5. Schematic representation of the charging process in electrodes based on the MWCNT|MnO_x@AgO_y composite, as well as a mixture of the composite and carbon black.

manganese and silver oxides, which are interconnected only in some areas with a sufficiently high contact resistance. As a result, during the charging process (when a positive potential is applied to the platinum current collector), only the layer of material located near the current collector is actively charged, and the potential value of the upper layers decreases due to the voltage drop in high-resistivity areas; consequently, the intensity of the redox reactions decreases. In the case of the combined electrode consisting of a mixture of the composite and highly dispersed CB, the composite agglomerates are distributed in a fairly dense CB matrix with a high electrical conductivity and a high porosity at the same time, providing good permeability for the electrolyte. Thus, in the „combined" electrode during charging, the decrease in potential with increasing distance from the current collector will be less significant, which, in turn, ensures a more „efficient" proceeding redox reaction on the surface of the composite agglomerates distributed in the CB matrix. The morphology of the „combined" electrode can also provide an increase in the contact area of the active component (composite agglomerates) with the electrolyte.

4. Conclusion

SEM, EDX, XPS, CV, as well as the galvanostatic charge-discharge methods were used to study the structure and electrochemical characteristics of the MWCNT|MnO_x@AgO_y composite produced by exposing MWCNT in an aqueous solution of potassium permanganate with the addition of silver nitrate (I). The XPS method showed that the resulting composite has a fairly high mass loading of manganese (~ 12 at.%), which is present predominantly in the form of MnO_2 oxide. Silver in the composite is present in the form of Ag_2O oxide, which has higher electrical conductivity compared to manganese oxide. The concentration of silver in the composite according to XPS data is less than 1 at.%. The formed composite was studied as an electrode material for supercapacitors with an aqueous electrolyte (1 M Na_2SO_4). Analysis of the electrochemical characteristics showed that the composite has high electrochemical activity due to the proceeding redox reaction. However, due to insufficient electrical conductivity and morphological features, the specific capacity of the composite-based electrode decreases by more than 80% (from ~ 107 to 20 F/g) with an increase in the discharge current density from 0.1 to 1.0 A/g. Combining the composite with highly dispersed commercial CB (Printex XE2-B) in various mass ratios makes it possible to produce electrodes with more optimal capacitive characteristics. The specific capacitances of the combined electrodes, measured by the galvanostatic charge−discharge method, are $\sim 145-130$ F/g at a current density of 0.1 A/g. The decrease in specific capacitance with an increase in the discharge current density to 1.0 A/g ranges from $\sim 47-35$% depending on the CB content in the electrode. The self-discharge rate of combined electrodes is $\sim 40-60$ mV for 4 h when measured in a three-electrode cell. Analysis of the morphology and electrical characteristics showed that the best capacitive characteristics of the combined electrodes are due to higher electrical conductivity, as well as the morphology of the electrodes, which ensures more efficient charge accumulation due to the proceeding redox reaction reactions. The results obtained in this study can be used in the development of new efficient electrode materials for supercapacitors.

Funding

This study was supported financially by grant No. 23-22-10030 from the Russian Science Foundation, https://rscf.ru/project/23-22-10030/. Part of the study related to the structure of the composite using the SEM method was carried out within the framework of the state assignment of the Omsk Scientific Center of the Siberian Branch of the Russian Academy of Sciences (state registration number of the project 121021600004-7). The study was performed using the equipment at the Omsk Regional Shared Equipment Centre of the Siberian Branch of RAS.

Conflict of interest

The authors declare that they have no conflict of interest.

References

[1] J. Wang, F. Kang, B. Wei. Prog. Mater. Sci. **74**, 51 (2015).
[2] M.E. Sahin, F. Blaabjerg, A. Sangwongwanich. Energies **15**, 674 (2022).
[3] A.G. Olabi, Q. Abbas, M.A. Abdelkareem, A.H. Alami, M. Mirzaeian, E.T. Sayed. Batteries **9**, *1*, 19 (2023).
[4] N.R. Chodankar, H.D. Pham, A.K. Nanjundan, J.F.S. Fernando, K. Jayaramulu, D. Golberg, Y.-K. Han, D.P. Dubal. Small **16**, *37*, 2002806 (2020).
[5] Q.-Z. Zhang, D. Zhang, Z.-C. Miao, X.-L. Zhang, S.-L. Chou. Small **14**, *24*, 1702883 (2018).
[6] N. Nagarajan, H. Humadi, I. Zhitomirsky. Electrochim. Acta **51**, 3039 (2006).
[7] J.H. Kim, C. Choi, J.M. Lee, M.J. Andrade, R.H. Baughman, S.J. Kim. Sci. Rep. **8**, 13309 (2018).
[8] V. Gaubert, H. Gidik, N. Bodart, V. Koncar. Sensors **20**, *6*, 1739 (2020).
[9] S.N. Nesov, Yu.A. Stenkin, P.M. Korusenko, V.V. Bolotov, S.A. Matyushenko. FTT **65**, *8*, 1440 (2023). (in Russian).
[10] S.W. Zhang, G. Chen. Energy Mater. **3**, 186 (2013).
[11] A. Mukherji, L. Wang, J. Zou, G.J. Auchterlonie, G.Q. Max Lu. J. Nanosci. Nanotechnol. **8**, 2011 (2008).
[12] A. Natoli, B.I. Arias-Serrano, E. Rodríguez-Castellón, A. Zurawska, J.R. Frade, A.A. Yaremchenko. Materials **14**, 641 (2021).
[13] N. Yu, H. Yin, W. Zhang, Y. Liu, Z. Tang, M.-Q. Zhu. Adv. Energy Mater. **6**, 1501458 (2016).
[14] R.R. Unocic, L. Baggetto, G.M. Veith, J.A. Aguiar, K.A. Unocic, R.L. Sacci, N.J. Dudney, K.L. More. Chem. Commun. **51**, *91*, 16377 (2015).

[15] V.V. Shunaev, N.G. Bobenko, P.M. Korusenko, V.E. Egorushkin, O.E. Glukhova, Int. J. Mol. Sci. **24**, 1296 (2023)
[16] V.I. Sysoev, A.V. Okotrub, A.V. Gusel'nikov, D.A. Smirnov, L.G. Bulusheva. Phys. Status Solidi B **255**, 1700267 (2018).
[17] NIST X-ray Photoelectron Spectroscopy Database. (https://srdata.nist.gov/xps/).
[18] L. Yu, George Z. Chen. Electrochem. Energy Rev. **3**, 271 (2020).
[19] P.M. Korusenko, S.N. Nesov, A.A. Iurchenkova, E.O. Fedorovskaya, V.V. Bolotov, S.N. Povoroznyuk, D.A. Smirnov, A.S. Vinogradov. Nanomaterials **11**, *9*, 2163 (2021).
[20] D.G. Gromadskyi, J. Chem. Sci. **128**, 6 (2016).
[21] R. Vicentini, L.M. Da Silva, E.P. Cecilio Junior, T.A. Alves, W.G. Nunes, H. Zanin. Molecules **24**, 1452 (2019).

Translated by Y.Alekseev